https://dx.doi.org/10.1016/j.jcsr.2019.105729

Experimental investigation on steel-tube-confined-concrete stub column with different cross-section shapes under uniaxial-compression

Jiong-Yi ZHU and Tak-Ming CHAN*

Department of Civil and Environmental Engineering, The Hong Kong Polytechnic University, Hung Hom, Hong Kong

*tak-ming.chan@polyu.edu.hk

Abstract

An experimental investigation on steel tube confined concrete (STCC) stub columns with circular, square and octagonal cross-section shapes under monotonic axial compression was conducted. Different concrete grades were examined with measured compressive cylinder strengths ranging from 38 MPa to 112 MPa. The nominal yield stress of the steel tube was 355 MPa. The load capacity, load-axial shortening curves and axial-hoop strain behaviour of the STCC stub columns are compared to that of the counterparts, concrete filled steel tubes (CFST), with different cross-section shapes based on the same material and geometrical properties. Comparisons indicated that the load capacity of STCC stub columns are very close to that in the CFST with circular and octagonal cross-sections, while the performance of square STCC is not as good as the CFST counterparts due to low effectiveness of confinement. According to the experimental results of lateral behaviours of STCC, CFST and plain concrete columns, it was concluded that with very high strength concrete (cylinder strength over 100 MPa), the axial performance of STCC stub columns is better than that in CFST. A design assessment was also conducted on STCC stub columns and shows that the current design formulae for load capacity of CFST are also applicable to that of STCC stub columns.

Keywords: Steel tube confined concrete columns; Octagonal cross-section shape; High strength concrete; Confinement; Cross-section resistance; Design method.

1. Introduction

One of the advantages of traditional CFST is that the concrete strength could be enhanced by the confining pressure from steel tube. However, in traditional CFST columns, the external axial compression is resisted by both concrete core and steel tube. With the presence of the longitudinal axial stress in the steel tube, the lateral stress cannot reach the yield stress to provide effective confining pressure. O'Shea and Bridge [1] indicated that there were three loading cases for the CFST. When the loading case is changed, the effect of confinement is also significantly changed. The three types of loading cases for CFST are namely, (a) loading on steel tube only; (b) loading on concrete core only and (c) loading on both steel tube and concrete core as illustrated in Figure 1. For case (a), there is no confinement for the concrete core because the steel tube expands in hoop direction due to the Poisson's ratio, which resulting in a separation of the steel tube and the concrete core. For case (b), as the load is only imposed on the concrete core, the steel tube is acting as a confining jacket to provide efficient confinement which significantly increases the compressive strength of the concrete core. For case (c), as the load is acting on the steel tube and the concrete core simultaneously, the confining pressure is only imposed when the concrete core expands more than the steel tube. Meanwhile the axial stress in the steel tube may reduce the hoop stress, resulting to a lower confining pressure compared to case (b). According to the experimental results, O'Shea and Bridge [1] concluded that the extra enhanced strength of concrete core in case (b) can even make up the loss of load capacity from the steel tube in case (c). The concept of steel tube confined concrete (STCC) was firstly proposed by Tomii [2] and followed by Yamamoto et al. [3], O'Shea and Bridge [1], Johansson and Gfylltoft [4], Fam et al. [5], Han et al. [6], Qi et al. [7] and Liu et al. [8] aim to disconnect the steel tube at beam-column joint to eliminate the axial stress in the steel tube from external force as shown in Figure 2, where only the concrete core is connected to the beam at the beam-column connection. Qi et al. [7] tested 14 circular and 15 square STCC stub columns, and the results showed that the STCC stub columns (load case b) can achieve higher load capacity than the commonly used CFST stub columns (load case c). Liew and Xiong [9] also investigated the axial behaviour of STCC stub columns. They observed a larger relative slip between the concrete core and the steel tube in their STCC specimens compared to CFST stub columns. Liew and Xiong [9] also indicated the confining pressure between concrete core and steel tube generates significant friction which transfers the external axial load from the concrete core to the steel tube and finally the concrete core and the steel tube were loaded simultaneously again. Later Liu et al. [10] investigated the effect of friction in circular STCC stub columns, a theoretical model was developed to capture the transferred axial stress in steel tube. Recently, Liu et al. [8] extended the research on STCC stub columns to high strength concrete and observed that the STCC stub columns with high strength concrete show a higher brittleness compared to the normal strength concrete counterparts. Based on the above-mentioned literature, the interaction between the concrete core and the steel tube in STCC stub columns can be concluded as follows: At the first stage of loading, a small part of the axial load was transferred from the concrete core to the steel tube because of the interfacial bond stress. Then as the applied load increases, the bond stress is insufficient and slip between the concrete core and the steel tube occurs, meanwhile the concrete core starts to expand and the confining pressure increases as well as the friction; finally the concrete core and the steel tube are loaded together again due to the large interfacial friction caused by the confining pressure. Octagonal cross-section shape is a new cross-section shape that can be used in CFST columns [11-14]. Previous study indicates that this cross-section shape combines the merits of circular cross-section (concrete confinement) and square cross-section (ease of fabricating beam-column connection) [11]. However, no research has been conducted on octagonal STCC to date and the effect of confinement in STCC with octagonal cross-section shape should be studied. In summary, limitations were found in current investigations of STCC stub columns under compression, especially related to octagonal section and high strength concrete. Besides the design formula of load bearing-capacity of STCC stub columns is not covered in current design codes, thus more test data and design recommendation should be developed. In this paper, research on STCC stub columns has been extended to octagonal STCC stub columns, with a comparison to the traditional CFST stub columns under the same material and geometrical properties, high strength concrete with cylinder strength higher than 100 MPa was also used and the experimental results were compared with the current design formulae of CFST.

2. Experimental investigation

2.1 Specimens

For this investigation, 19 STCC stub columns with circular, octagonal and square section were prepared. To present a comparative investigation, the material properties and fabrication method of the steel tube in STCC specimens were consistent with the complementary experimental works in octagonal CFST from the authors [11]. The steel tubes were fabricated with the cold-forming method where the virgin steel plates were bent by the press-braking process to form two half-section tubes and then both the half-section tubes were welded together. The concrete cores of STCC specimens were also cast at the time with the CFST specimens in Zhu and Chan [11]. Three concrete grades were used with measured compressive cylinder strength of 38, 80, and 112 MPa respectively and the yield stress of the steel tubes ranged from 413 MPa to 485 MPa. The nominal thickness of the steel tubes is 6 mm and the dimension of the cross-sections can be found in Figure 3 and Table 1. The heights of all the specimens were 695 mm. The material properties of steel and concrete are summarized in Table 2. Tensile coupons extracted from the corner and the flat regions of steel tubes were tested and the weighted average yield stresses are summarized in Table 2 where f_y and f_u are the yield stress and ultimate stress of steel tube respectively and E is the Young's modulus of steel tube. The tensile test procedure followed the current design and literature guidelines [14-17]. Compressive tests of standard concrete cylinders as well as plain concrete stub columns with the same size as the concrete core in STCC specimens were also conducted [11, 18] and the average results from each concrete grade are shown in Table 2 where f_{co} and $f_{co,c}$ are the compressive strength of standard concrete cylinders and plain concrete stub columns respectively. The details of the compressive tests of plain concrete stub columns can be found in the authors previous study [11]. The STCC specimens were labelled as SXY-Z where S stands for STCC to differentiate from CFST (C), X stands for concrete grade, Y stands for cross-section shape where C stands for circular section, O stands for octagonal section and S stands for square section, Z stands for the number of repeated specimens, the specimen's labels which start with P stand for the plain concrete columns without steel tube.

2.2 Stub column tests

The stub column tests were conducted under a compression machine with a load capacity of 10000 kN. To avoid the axial stress in the steel tube from the external compression, loading plates with the same cross-section dimension of the concrete core were machined. Two fabricated loading plates were placed at both ends of the specimen as shown in Figure 4(a). The loading plates were machined slightly smaller than the dimensions of the concrete cores to avoid any friction between the inner surface of the steel tubes and the loading plates. The gap between the edge of the loading plate to the inner edge of the steel tube is about 2 mm and the tolerance of the dimensions is less than 1 mm. Four LVDTs were placed around the specimen with 90 degrees apart to record the axial shortening. Strain gauges with 15% strain limits were used to measure both the axial strain and the hoop strain at the mid-height of the columns. Steel rings were mounted at the both ends of the columns to prevent premature failure at column ends. The test set-up and the arrangement of strain gauges and LVDTs are shown in Figure 4(b) and 4(c) which are consistent with the arrangement in stub column tests of CFST in Zhu and Chan [11].

2.3 Load capacity

The load capacities of stub column tests are shown in Table 3. f_y and f_{co} are the yield strength of steel tube and the cylinder strength of concrete core respectively. $N_{u,s}$ is the load capacity of the STCC specimens and N_p is the load capacity of the plain concrete columns without any external steel tube. ξ is the confinement ratio which is defined as the plastic resistance of steel tube divided by the plastic resistance of concrete core, i.e. A_sf_y/A_cf_{co}. To investigate the increase of load capacity from confinement, the load capacities of the STCC specimens were compared with the original load capacities of the plain concrete columns which have the same geometrical and material properties of the concrete core inside the STCC specimens. Table 3 shows the enhancement percentage of the load capacity of the concrete core after being confined by the steel tube which is very high in the specimens with circular cross-section ($N_{u,s}/N_p$ up to 324% in specimen S30C-2). For octagonal STCC, similar percentage of enhancement in load capacity is found when compared to the circular STCC columns, which is about 215% ($N_{u,s}/N_p$=315%). It should be noted that the enhancement in the load capacity is not only from the effect of confinement, but also from the interfacial friction which transfers part of the external axial load from the concrete core to the steel tube and results in a higher load bearing compacity due to the contribution of the steel tube. As the cross-section shape changes from circular section to octagonal section, no significant reduction on the enhancement of load capacity was found, the maximum reduction is only about 16%, however, significant decrease of the enhancement ratio, $N_{u,s}/N_p$, was found when the cross-section shape changes to square where the maximum and the minimum enhancement are about 85% ($N_{u,s}/N_p$=185%, specimens S30S-1) and 8% ($N_{u,s}/N_p$=185%, specimens S80S-1) respectively. The interpretation is the poor confinement effectiveness of square section. An obvious trend was found which shows the enhancement of load capacity decreases with the decrease of confinement ratio.

2.4 Stress-strain relationship

The stress-strain curves of the STCC specimens are shown in Figure 5. Axial and hoop strains in the steel tube of STCC stub columns were recorded by the strain gauges and the overall axial strain was recorded by the four LVDTs, the arrangement of strain gauges and LVDTs are shown in Figure 4(c). The averaged axial stress of the concrete column was calculated from the applied load divided by the cross-sectional area of the concrete core because the loading plates are only in contact with the concrete core. The curves of those specimens with high confinement ratio (with measured concrete cylinder strength of 38 MPa) show hardening behaviour in their stress-strain curves while for those curves of specimens with lower confinement ratio (with measured concrete cylinder strength 80 and 112 MPa) softening behaviour was found after peak load. From the comparison between the specimens with different cross-section shapes, it can be found that the initial slopes of specimens with different cross-section shapes are almost identical, and that the specimens with square section are those firstly approach their ultimate strength due to their poor confinement effectiveness. The curves of specimens with circular and octagonal section are very similar, which means the confinement effects in these two sections are close to each other. It should be noted that unexpected failure in welding seam was found in circular specimens S30C-1 and S30C-2 which resulted in uncompleted stress-strain curves in Figure 5(a). Due to the confinement, the highest hoop stress was anticipated in circular specimens. The lower confinement effect in octagonal and square STCC specimens when compared to that in circular specimens was due to the non-uniform confinement between flat sides and corners. The axial stress-hoop strain relationships of octagonal and square specimens are shown in Figure 6 and Figure 7. The axial strain and hoop strain are the averaged values from strain gauges (see Figure 4(c)). It can be found that the hoop strain at the flat sides is larger than that in the corners in octagonal STCC specimens which is due to the lack of confinement in the flat sides which allows the concrete core to expand more than that at the corners. In axial stress to hoop strain curves of square specimens, compressive hoop strains were found in the corner region. This can be attributed to the relatively large expansion of the concrete core in the flat region which caused a bending stress at the sharp corner. The bending stress at outer surface of steel tube is compressive in nature. Figure 8 shows the axial stress-hoop strain curves of circular STCC specimens. The lateral behaviours before peak load at four locations of the circular STCC columns are consistent due to a uniform confinement.

2.5 Failure mode

Failure modes of STCC specimens are shown in Figure 9. Two typical failure modes were found. Specimens such as S30O-2 and S30S-1 show an outward buckling failure in the steel tube. However, some of the specimens failed at the welding seam of steel tube unexpectedly due to the large hoop stress. Failures at the welding seam happened after the peak load in most of the specimens except specimens S30C-1 and S30C-2. After removing the external steel tube from the specimen S30O-2 as shown in Figure 10, it was found that the local buckling of the steel tube occurred with the local crushing of the concrete core at the same level of the column height.

3. Comparison with CFST

To compare the axial performance between STCC and CFST stub columns, the only difference between the CFST specimens presented in Zhu and Chan [11] and the current STCC specimens is that the loading plates have no contact with the steel tube in STCC specimens to ensure there is no external axial load on the steel tube. The specimens of STCC stub columns in this paper have identical geometrical and material properties to the CFST specimens presented in Zhu and Chan [11] in order to eliminate the experimental deviations from cross-sectional dimensions and material strength, and to ensure that a consistent comparative investigation can be presented.

3.1 Load capacity

Table 4 shows the comparison between load capacities of STCC and CFST specimens, where the specimens with label S indicates the STCC specimens and C indicates the CFST specimens from Zhu and Chan [11]. $N_{u,s}$ and $N_{u,c}$ are the load capacities of STCC and CFST specimens respectively. It should be noted that in Table 4, an average test value from the repeated specimens is used. The ratio, $N_{u,s}/N_{u,c}$ shows that the load capacities of STCC and CFST specimens are very close (within 5%) for those specimens with circular and octagonal sections and with measured concrete cylinder strength of 38 MPa and 80 MPa. This observation indicates that the applied axial stress was transferred from the concrete core to the steel tube because of the large friction, and the biaxial stress in steel tube of STCC will eventually be the same as that in CFST which result in a similar load capacity. This observation is consistent with the finding in Liew and Xiong [9]. However, in the specimens with a square section and specimens with a very high measured cylinder strength (112 MPa), the difference of load capacities between STCC and CFST becomes larger. In the specimens with a measured concrete cylinder strength of 112 MPa, the load capacity of STCC is 13% and 8% higher than that in the CFST counterpart with circular and octagonal cross-section shapes respectively. For those square specimens, the load capacity of the STCC is much lower than the that in the CFST, which is only about 70%, 61% and 62% for specimens with measured concrete cylinder strengths 38 MPa, 80 MPa and 112 MPa respectively. It is because the low confinement effectiveness of square section results in a poor capacity enhancement in the concrete core (see Table 3) and the load transferred from the concrete core to the steel tube is also minor. The comparison of load-axial shortening is shown in the following section.

3.2 Load-axial shortening behaviour

The comparison of load-axial shortening behaviours of STCC and CFST is shown in Figure 11. As the load-axial shortening curves between repeated specimens show a very good consistency (see Figure 5), for each configuration only a curve of one repeated specimen was shown in Figure 11. Significant difference was found between the curves of square STCC and CFST for all three concrete grades, which is consistent with that observed for the load capacity, the poor confinement effect in square cross-section results in a lower load capacity as well as the load-shortening curve of STCC specimen. In Figure 11(a), the observed differences between STCC and CFST are similar for the specimens with circular (S30C and C30C) and octagonal (S30O and C30O) section. In the initial elastic stage, the stiffnesses of CFST specimens are much higher than those of STCC specimens because in the CFST specimen, the steel tube was bearing the axial load together with the concrete core which results in a larger value of *EA/L* where *E* and *A* are the elastic modulus and the cross-sectional area of the section respectively and *L* is the column length. As the load is approaching to the peak, the curves of CFST and STCC meet and overlap which is consistent with the explanation that at peak load, the conditions of biaxial stress in steel tube of STCC and CFST are almost the same. A similar observation was found in the comparison of the curves of circular and octagonal STCC and CFST with measured cylinder strength 80 MPa. For the curves of circular and octagonal STCC and CFST with measured cylinder strength 112 MPa, a lower stiffness and a higher peak load were found in the STCC specimens which is consistent with the observation in the comparison of load capacity. This observation could be explained after comparing the axial-hoop strain relationship of STCC and CFST in the following section.

3.3 Axial-hoop strain relationship

In the comparison of load capacities and load-shortening curves of STCC and CFST, it was found that with very high concrete strength, the performance of the STCC stub columns is better than that in the CFST columns. To further explain this observation, the axial-hoop strain relationships of STCC and CFST specimens as well as plain concrete stub columns without steel tube are shown in Figure 12. It should be noted the axial-hoop strain curves of STCC and CFST in Figure 12 are collected from strain gauges at the surface of the steel tube of the specimens with circular cross-section for each concrete grade. It is known that the hoop strain in the steel tube is larger than that in the concrete core in CFST at the initial stage because the Poisson's ratio of steel is larger than that of concrete. With an increase in load, the hoop strain of the concrete core (unconfined) increases rapidly while approaching its compressive strength and the contact of the steel tube and the concrete core as well as the confinement starts. In this comparison the collected axial-hoop strain relationship of plain concrete stub columns is used to represent the lateral behaviour of the concrete core inside the CFST before the contact happened. As shown in axial-hoop strain relationship of plain concrete and CFST in Figure 12(a) and Figure 12(b), the intersection of the curves could be defined as the moment when the contact of the steel tube and the concrete core happens. However, due to the brittleness of very high strength concrete, the expansion of the concrete core in the lateral direction is not as much as that in normal strength concrete which results in the failure of concrete taking place before the contact as shown in Figure 12(c). This observation indicates that the effect of confinement in CFST with very high strength concrete may be reduced by the pre-damaged concrete core before the confinement happens. However, in STCC stub columns this problem could be avoided as the confinement begins as soon as the load is applied because there is no external axial stress in steel tube. As Figure 12 shows, the magnitude of hoop strain of STCC is much smaller than CFST and plain concrete columns because of the effect of confinement. Therefore, it can be concluded that when very high strength concrete (e.g. concrete cylinder strength higher than 100 MPa) is used, STCC stub columns are superior over CFST stub columns in load bearing capacity because in CFST, the concrete core may be damaged before the steel tube confines it.

4. Design assessment

In current design guidelines such as Eurocode 4 [19] and American code [20, 21], there is no design specification on the load capacity of STCC stub columns. However, from the experimental observations, the load capacity of STCC specimen is almost the same as that in CFST specimens which is consistent with the conclusions from the existing literature [6,9], although in stub columns with very high strength concrete, it was found that the load capacity of STCC is higher than that of CFST, the observed maximum difference is 13%. Therefore, in this assessment, the current design formulae on the load capacity of CFST were assessed for the STCC stub columns with circular, octagonal and square section. Additionally, the design method for STCC stub columns with circular section from Liu *et al.* [10] was also assessed. It should be noted that the concrete strength $f_{co,c}$, the compressive strength of plain concrete with the same scale as the concrete core, was used in this assessment from Table 3 to account for the reduction of compressive strength of high strength concrete (Zhu and Chan [11]).

4.1 Eurocode 4 [19]

Eurocode 4 [19] provides two formulae for the load capacity of CFST. One is a general formula where the cross-section shape of CFST is not specified. The other one is for CFSTs with a circular cross-section which considers the effect of confinement. These two formulae are shown as follows.

$$N_d = A_s f_y + A_c f_{co} \quad \text{for general section} \tag{1}$$

$$N_d = \eta_a A_s f_y + A_c f_{co}\left(1+\eta_c \frac{t}{d}\frac{f_y}{f_{co}}\right) \quad \text{for circular section} \tag{2}$$

In the case of uniaxial load:

$$\eta_a = 0.25\left(3+2\bar{\lambda}\right) \leq 1$$

$$\eta_c = 4.9 - 18.5\bar{\lambda} + 17\bar{\lambda}^2 \geq 0 \quad (3)$$

$$\bar{\lambda} = \sqrt{\frac{N}{N_{cr}}} \quad (4)$$

where N_d is the design value of load capacity, N_{cr} is the elastic critical force, A_s and A_c are the cross-sectional area of steel tube and concrete core respectively. η_a and η_c are the modification factors on steel tube and concrete core related to confinement of concrete, t is the thickness of steel tube and d is the outer diameter of circular CFST. In the assessment, Eq. (1) was used for the STCC specimens with square section and Eq. (2) was used for the specimens with circular section. As there is no specification of design formula on load capacity of octagonal CFST, the design method proposed by Zhu and Chan [11] based on the current design formula in Eurocode 4 (Eq.2) with an equivalent circular section approach was used in the assessment, the design equation for octagonal STCC is shown as follows:

$$N_d = \eta_{a,Di} A_s f_y + A_c f_{co}\left(1 + 0.73\eta_{c,Di}\frac{t}{d}\frac{f_y}{f_{co}}\right) \quad (5)$$

where $\eta_{a,Di}$ and $\eta_{c,Di}$ are the modification factors based on the inscribed circular section of octagonal section.

4.2 American code [20, 21]

American codes [20, 21] provide a simple formula for CFST. It is suggested that the load capacity of CFST is given as the sum of the load capacity of the steel and concrete components. The beneficial effect of confinement for circular CFST is also considered. The design formulae are shown as follows

$$N_d = A_s f_y + 0.85 A_c f_{co} \quad \text{for general section} \quad (6)$$

$$N_d = A_s f_y + 0.95 A_c f_{co} \quad \text{for circular section} \quad (7)$$

In the assessment of American codes [20, 21], Eq. 6 was used for the square STCC test results and Eq. 7 was used for the circular STCC specimens. For octagonal cross-section, it has been found that the effect of confinement should be considered, thus in this assessment Eq. 7 (for circular section) was used for the octagonal STCC specimens.

4.3 Design method from Liu et al. [10]

Liu *et al.* [10] proposed a design method for the load capacity of circular STCC columns by developing a theoretical model of biaxial stress in steel tube based on the load transfer between concrete core and steel tube. The axial stress distribution in column height on steel tube which is determined by the friction between the concrete core and the steel tube is established according to the following equation in Liu *et al.* [10]:

$$\frac{\sigma_{a,s}}{f_y} = 0.36\left(\frac{\mu}{D}x\right)^3 - 1.49\left(\frac{\mu}{D}x\right)^2 + 2.07\left(\frac{\mu}{D}x\right) \tag{8}$$

where $\sigma_{a,s}$ is the axial stress at the selected section in column height, x is the distance between the selected section and the end of the column. μ is the friction coefficient between the steel tube and the concrete core which is taken as 0.3 suggested by Liu *et al.* [8] and Liu *et al.* [10]. Then based on von Mises yielding criterion, the hoop stress in steel tube could be obtained.

$$\left(\sigma_{a,s}\right)^2 + \left(\sigma_{h,s}\right)^2 - \left(\sigma_{a,s}\sigma_{h,s}\right) - f_y^{\,2} = 0 \tag{9}$$

where $\sigma_{h,s}$ is the hoop stress in steel tube. With the hoop stress in steel tube, the lateral confining pressure on the concrete core in circular STCC could be obtained using the following equation:

$$f_l = \frac{2\sigma_{h,s}t}{D-t} \tag{10}$$

With the confining pressure f_l, Liu *et al.* [10] suggested that the formula for the compressive strength of confined concrete core from Richart *et al.* [22] could be used. The equation is shown as follows:

$$f_{cc} = f_{co} + 4.1f_l \tag{11}$$

Finally, the sectional capacity of STCC stub columns, $N_{u,s}$, can be calculated as:

$$N_d = \sigma_{a,s}A_s + \left(f_{co} + 4.1f_l\right)A_c \tag{12}$$

It should be noted that the design method of Liu *et al.* [10] is only applicable for STCC stub columns with circular section. To apply this design method for octagonal STCC stub columns, a slight modification was made. Based on the investigation on the confinement effect between circular and octagonal CFST in Zhu and Chan [11], the confinement reduction coefficient k = 0.73 is incorporated in Eq. 12 and the modified design formula is shown as follows to capture the load capacity of octagonal STCC stub columns.

$$N_d = \sigma_a A_s + \left(f_{co} + k4.1f_l\right)A_c = \sigma_a A_s + \left(f_{co} + 3.0f_l\right)A_c \tag{13}$$

4.4 Assessment result

The results of the assessment are shown in Table 5 and Figure 13. The design formula from Eurocode 4 on load capacity of CFST shows a very good accuracy on the prediction of load capacity of circular STCC stub columns which could be seen from the average ratio between design and experimental result, $N_d/N_{u,s}$ while the proposed design method in Zhu and Chan [11] for octagonal CFST also could capture the load capacity of octagonal STCC stub columns with a slightly conservative prediction. The design formulae from ACI 318-11/AISC 360-16 underestimate the load capacity of circular and octagonal. For the square STCC stub columns, all the design codes overestimate the load capacity with a percentage up to 50% which indicates the poor axial performance of square STCC when compared to traditional CFST. The design method proposed by Liu *et al.* [10] shows a good agreement with the experimental results for both circular and octagonal STCC stub columns. It should be noted that all the design formulae provide a higher prediction (higher $N_d/N_{u,s}$ ratio) in specimens with lower concrete strength (higher confinement ratio) and more conservative for these specimens with a higher concrete strength (lower confinement ratio) for both three different cross-section shapes. This observation is consistent with that found in the comparison investigation between the load capacity of STCC and CFST, the performance in section capacity of STCC stub columns is better than the CFST counterparts when the very high strength concrete was used.

5. Conclusions

This paper presents an experimental investigation on the steel tube confined concrete (STCC) stub columns with three different cross-section shapes, circular, octagonal and square section. In total, 19 STCC stub columns with three different concrete grades were tested under monotonic axial compression. The experimental results on STCC specimens were compared with the CFST specimens presented in Zhu and Chan [11] under consistent geometrical and material properties. The following conclusions were made based on the experimental study described in this paper:

1. The load capacities of STCC stub columns with circular and octagonal section are very close to those of the identical CFST stub columns. With higher concrete cylinder strength (higher than 100 MPa), a higher load capacity in STCC stub column was found. The initial stiffness of STCC stub columns under axial compression is lower than that in CFST columns and the overall axial strain at peak load is higher.
2. The load capacities and stress-strain relationships of octagonal STCC stub columns are very close to those of circular STCC, and the reduction of confinement effectiveness because the cross-section shapes from circular to octagonal shape is small in terms of the load capacity. The confinement effectiveness in square STCC is much lower than that in circular and octagonal STCC.
3. In assessing the design approaches, it was found that the approach using design formulae from Eurocode 4 [19] for the load capacity of circular CFST section can provide an accurate prediction for the load capacity of circular STCC stub columns. The modified design formula for octagonal CFST [11] can capture the load capacity of octagonal STCC stub columns with a slightly conservative prediction. The design approach from ACI 318-11/AISC 360-16 [20, 21] gives a very conservative prediction on the load capacity of STCC stub columns. The design method from Liu *et al.* [10] also gives accurate predictions on the current test results with a deviation of 5%. The design formulae of square CFST is not applicable for the square STCC since the load capacity is overestimated.

Acknowledgement

Authors are thankful to WoLee steel Co. Ltd. for supplying the test specimens. This paper was also supported by the research funding from the Construction Industry Council under the project "Application of Polygonal High Strength Concrete-filled Composite Column in Seismic-resistant Buildings in Hong Kong". The support from the Chinese National Engineering Research Centre for Steel Construction (Hong Kong Branch) at The Hong Kong Polytechnic University is also gratefully acknowledged.

References

[1] O'Shea, M. D., & Bridge, R. Q. (2000). Design of circular thin-walled concrete filled steel tubes. Journal of Structural Engineering, 126(11): 1295-1303.

[2] Tomii, M. (1985). Lateral Load Capacity of Reinforced Concrete Short Columns Confined by Stell Tube-Experimental Results of Preliminary Research. Proceedings of the International Specialty Confernce on Concrete-Filled Steel Tubular Structures, 19-26.

[3] Yamamoto, T., Kawaguchi, J., & Morino, S. (2002). Experimental study of scale effects on the compressive behavior of short concrete-filled steel tube columns. In Composite Construction in Steel and Concrete IV; 879-890.

[4] Johansson, M., & Gylltoft, K. (2002). Mechanical behavior of circular steel–concrete composite stub columns. Journal of structural engineering, 128(8), 1073-1081.

[5] Fam, A., Qie, F. S., & Rizkalla, S. (2004). Concrete-filled steel tubes subjected to axial compression and lateral cyclic loads. Journal of Structural Engineering, 130(4), 631-640.

[6] Han, L. H., Yao, G. H., Chen, Z. B., & Yu, Q. (2005). Experimental behaviours of steel tube confined concrete (STCC) columns. Steel and Composite Structures, 5(6), 459-484.

[7] Qi, H., Guo, L., Liu, J., Gan, D., & Zhang, S. (2011). Axial load behavior and strength of tubed steel reinforced-concrete (SRC) stub columns. Thin-Walled Structures, 49(9), 1141-1150.

[8] Liu, J., Teng, Y., Zhang, Y., Wang, X., & Chen, Y. F. (2018). Axial stress-strain behavior of high-strength concrete confined by circular thin-walled steel tubes. Construction and Building Materials, 177, 366-377.

[9] Liew, J. R., & Xiong, D. X. (2012). Ultra-high strength concrete filled composite columns for multi-storey building construction. Advances in Structural Engineering, 15(9), 1487-1503.

[10] Liu, J., Zhou, X., & Gan, D. (2016). Effect of friction on axially loaded stub circular tubed columns. Advances in Structural Engineering, 19(3), 546-559.

[11] Zhu, J. Y., & Chan, T. M. (2018). Experimental investigation on octagonal concrete filled steel stub columns under uniaxial compression. Journal of Constructional Steel Research, 147, 457-467.

[12] Fang, H., Chan, T. M., & Young, B. (2018). Material properties and residual stresses of octagonal high strength steel hollow sections. Journal of Constructional Steel Research, 148, 479-490.

[13] Chen, J., Chan, T. M., Su, R. K. L., & Castro, J. M. (2019). Experimental assessment of the cyclic behaviour of concrete-filled steel tubular beam-columns with octagonal sections. Engineering Structures, 180, 544-560.

[14] Zhu, J.Y., Chan, T.M. & Young, B., (2019). Cross-sectional capacity of octagonal tubular steel stub columns under uniaxial compression. Engineering Structures. 184:480-494.

[15] Huang Y., & Young B. (2014). The art of coupon tests. Journal of Constructional Steel Research. 96:159-75.

[16] CEN. (2016). EN ISO 6892-1, Metallic materials – Tensile testing. Part 1: Method of test at ambient temperature. CEN (European Committee for Standardization), Brussels.

[17] Ma J.L., Chan T.M. & Young B. (2016). Experimental investigation on stub-column behavior of cold-formed high-strength steel tubular sections. J Struct Eng; 142(5): 04015174.

[18] CEN. (2009). EN 12390-3, Testing hardened concrete: Compressive strength of test specimens. CEN (European Committee for Standardization), Brussels.

[19] CEN. (2004). EN 1994-1-1, Eurocode 4 – Design of steel structures – Part 1.1: General rules and rules for buildings. CEN (European Committee for Standardization), Brussels.

[20] ACI. (2014). ACI 318-14, Building code requirements for structural concrete and commentary. American Concrete Institute (ACI), Farmington Hills, MI.

[21] AISC (2016). AISC 360-16, Specification for Structural Steel Buildings, American Institute of Steel Construction (AISC), Chicago (IL), USA.

[22] Richart, F. E., Brandtzaeg, A., & Brown, R. L. (1928). A study of the failure of concrete under combined compressive stresses. University of Illinois at Urbana Champaign, College of Engineering. Engineering Experiment Station.

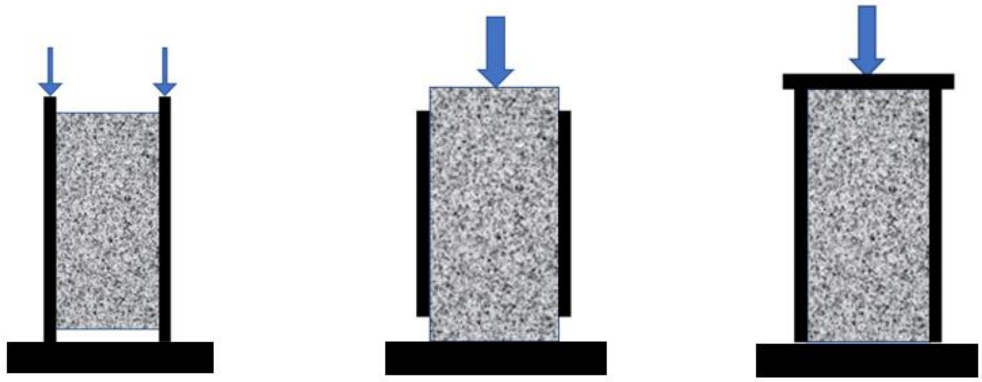

(a) Steel tube only (b) Concrete core only (c) Both steel tube and concrete core

Figure 1. Loading cases for CFST columns

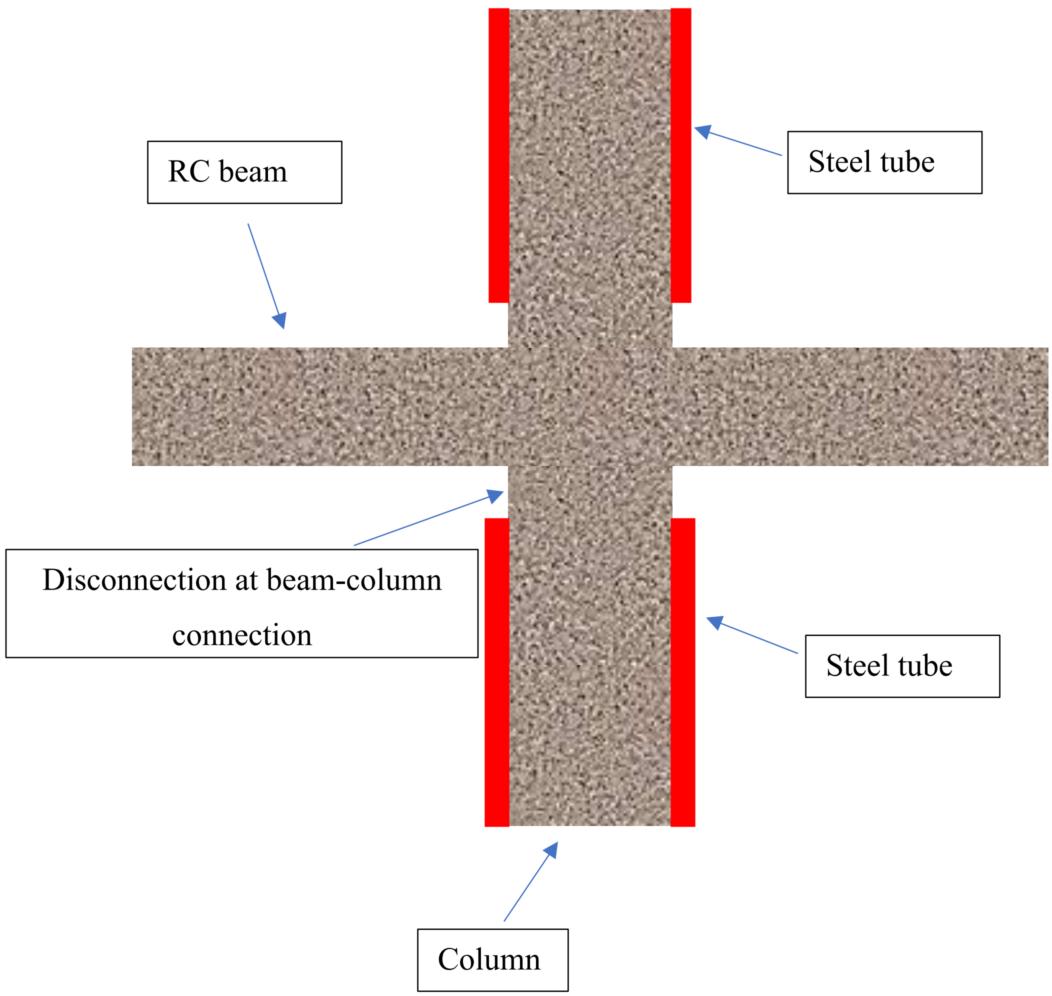

Figure 2. Schematic sketch of a beam-STCC column joint

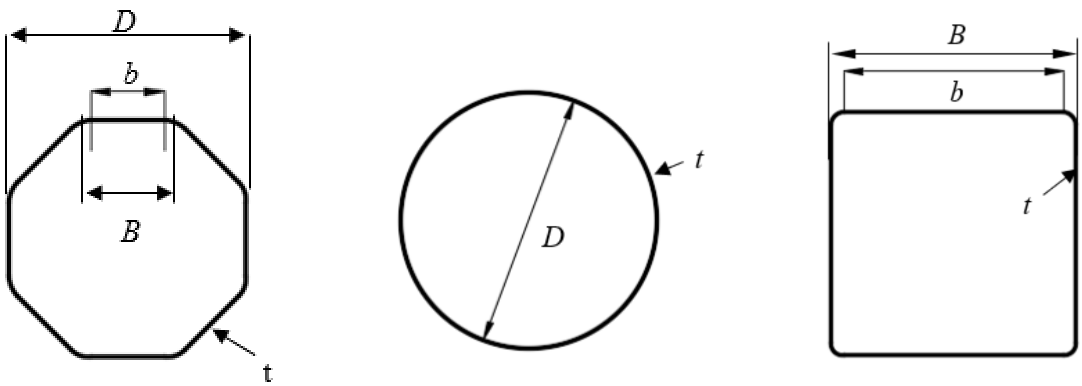

Figure 3. Dimensions of specimens

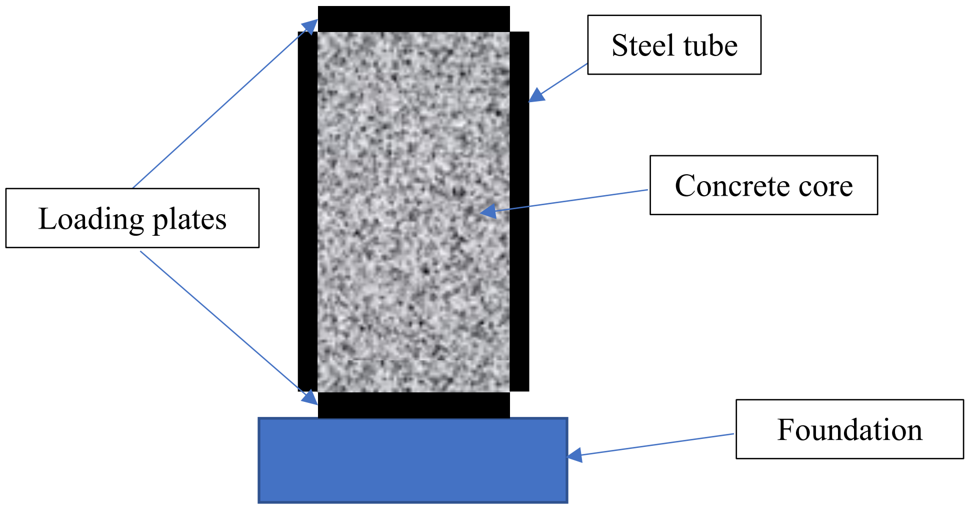

(a) Demonstration of loading case

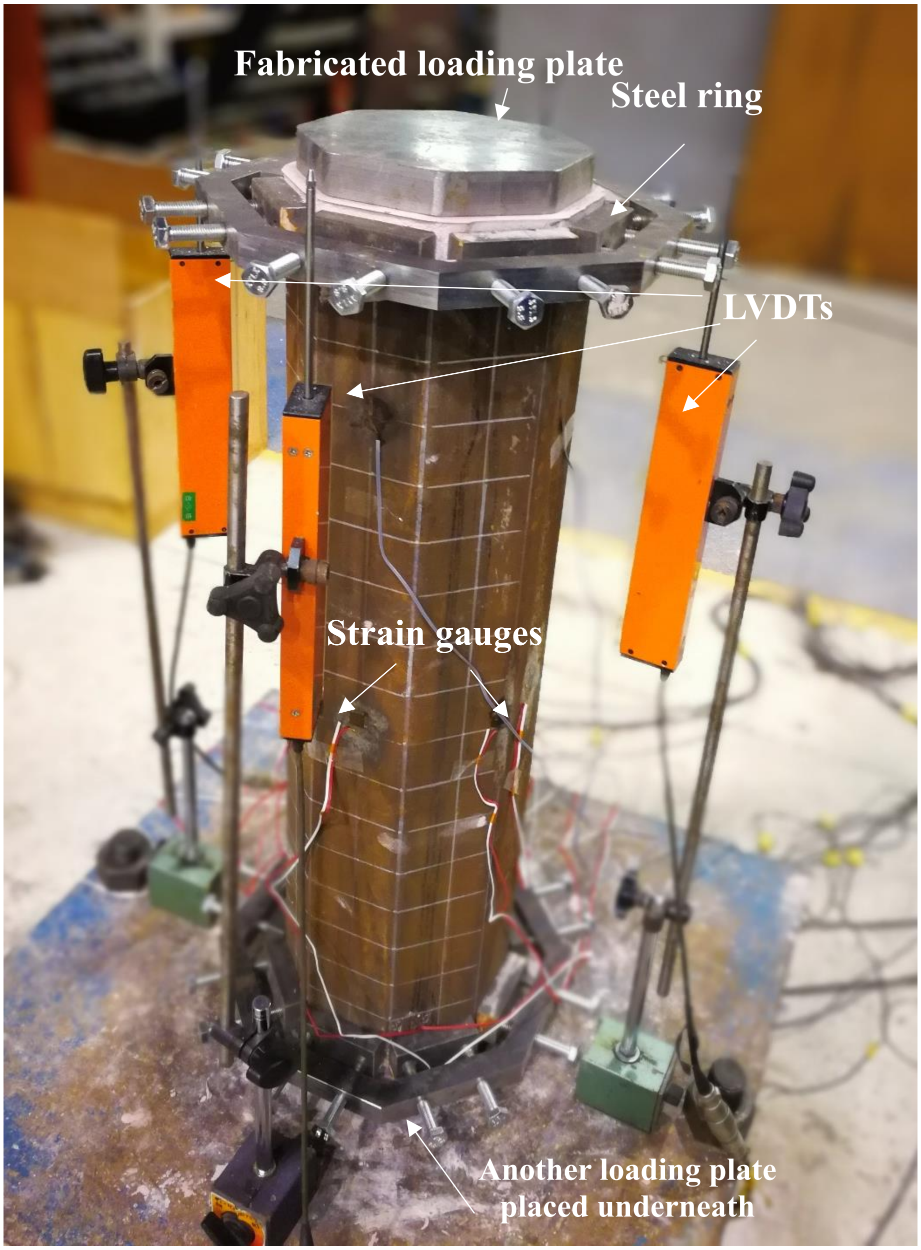

(b) Photo of test set-up

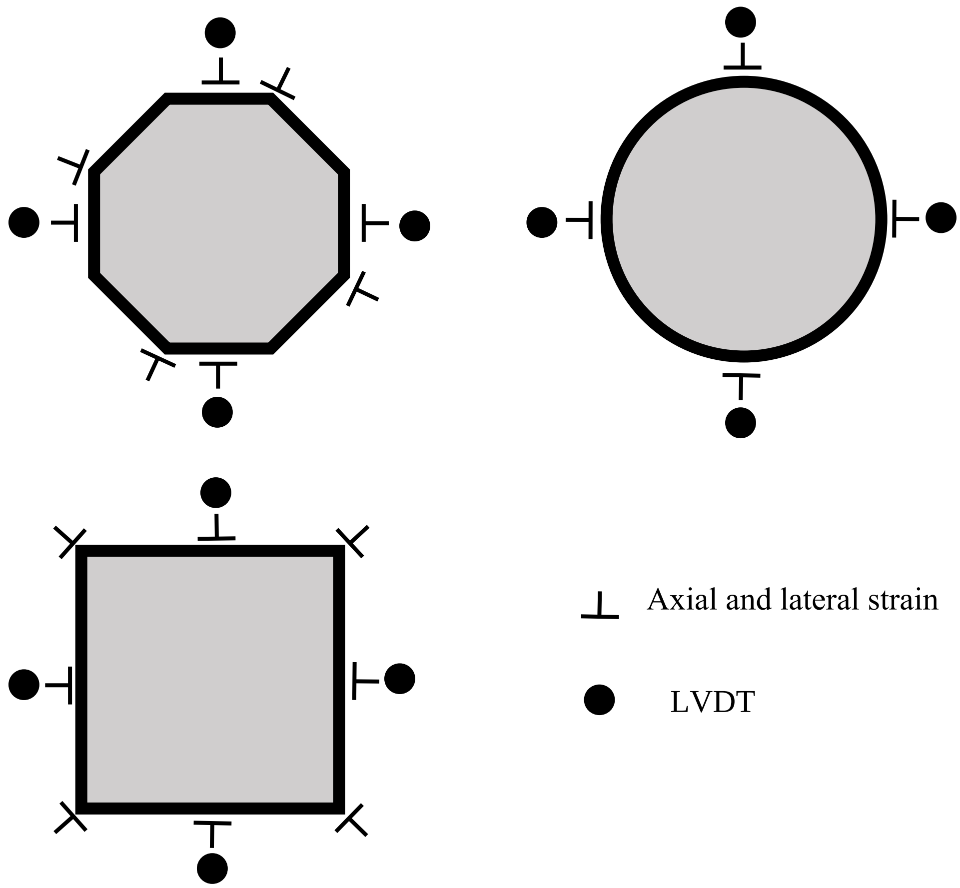

(c) Arrangement of instrumentation

Figure 4. Test set-up of STCC stub column

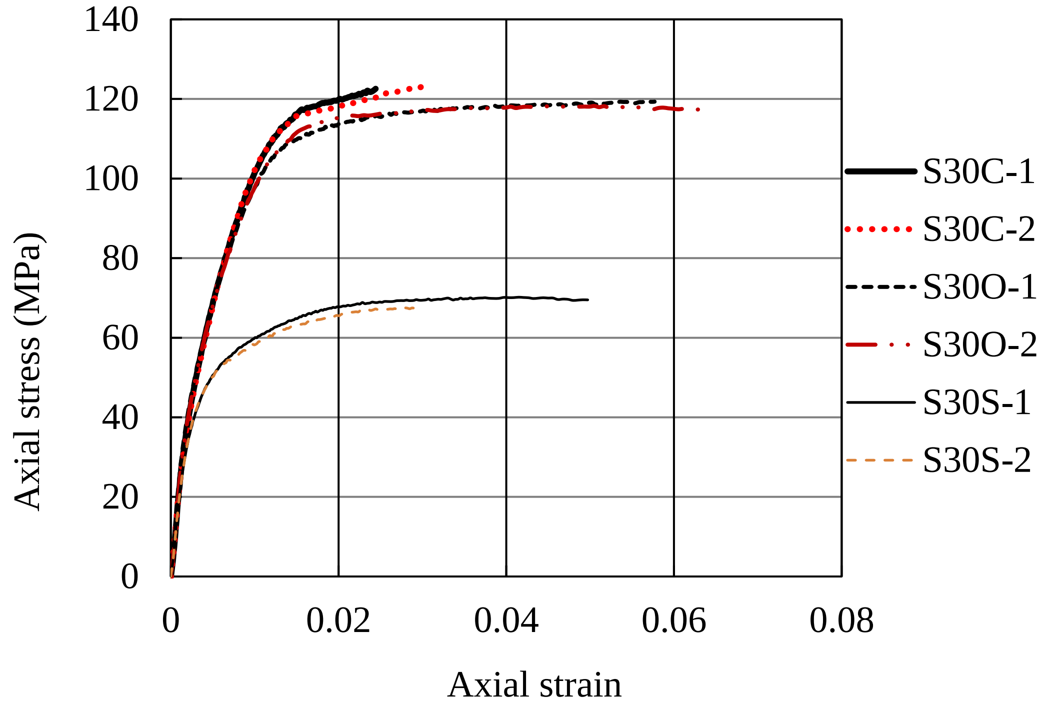

(a) Measured cylinder strength - 38 MPa

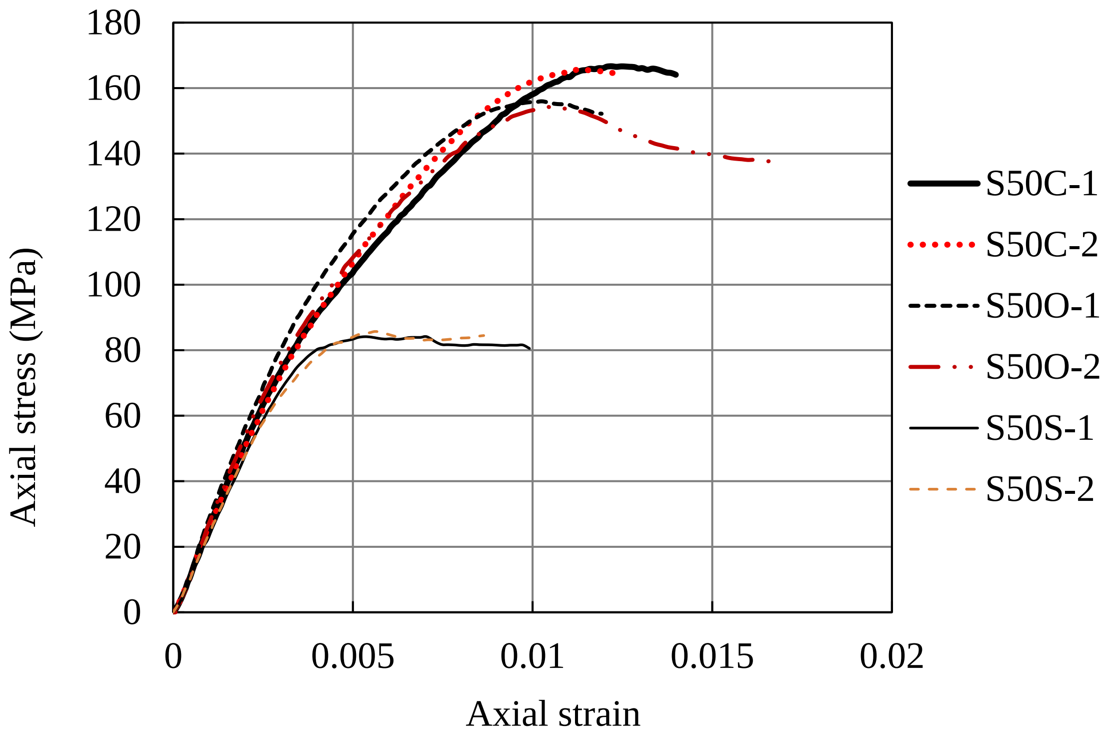

(b) Measured cylinder strength - 80 MPa

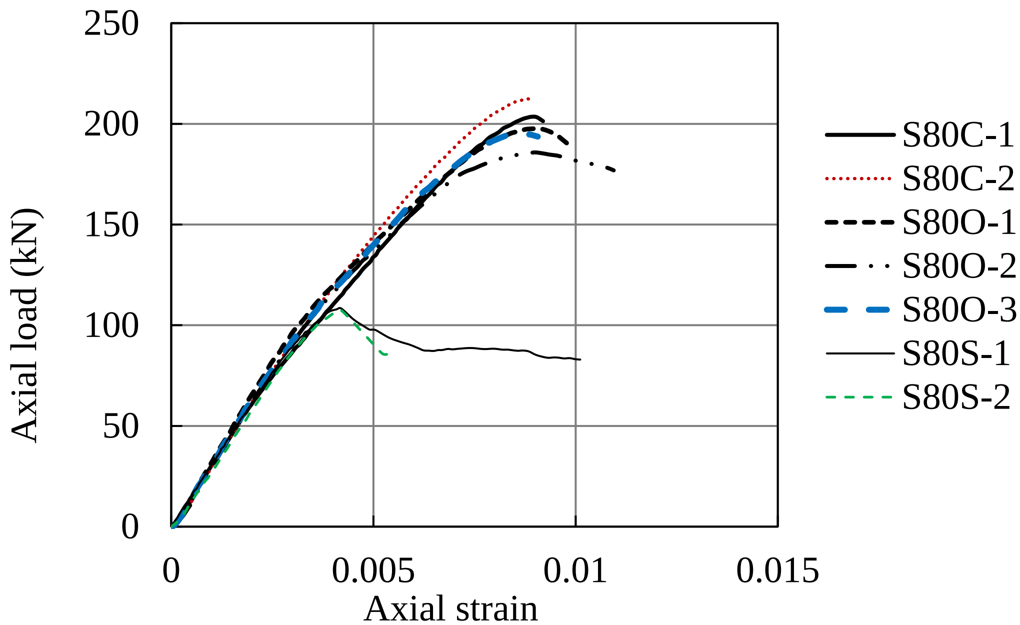

(c) Measured cylinder strength - 112 MPa

Figure 5. Axial stress-strain curves of the STCC specimens

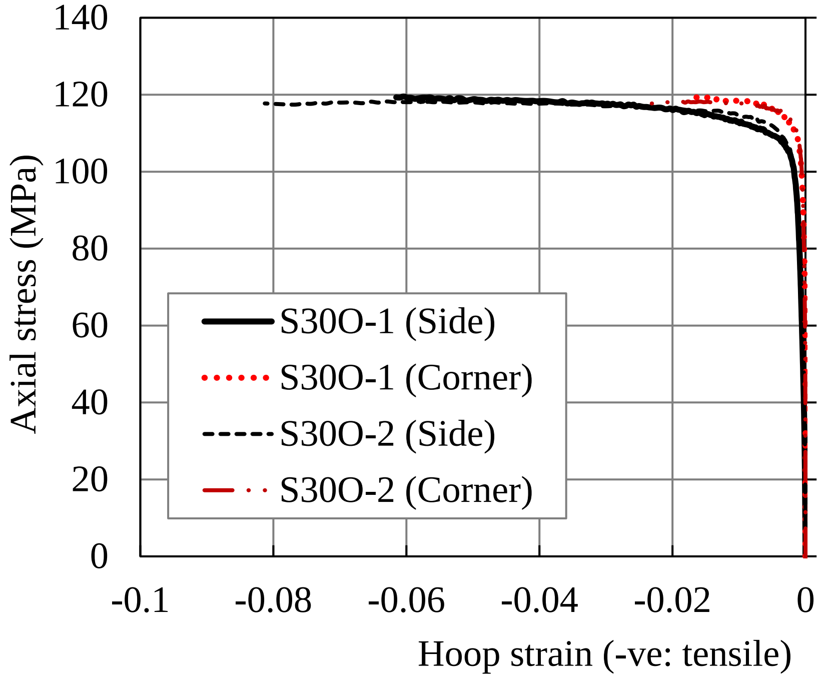

(a) Measured cylinder strength - 38 MPa

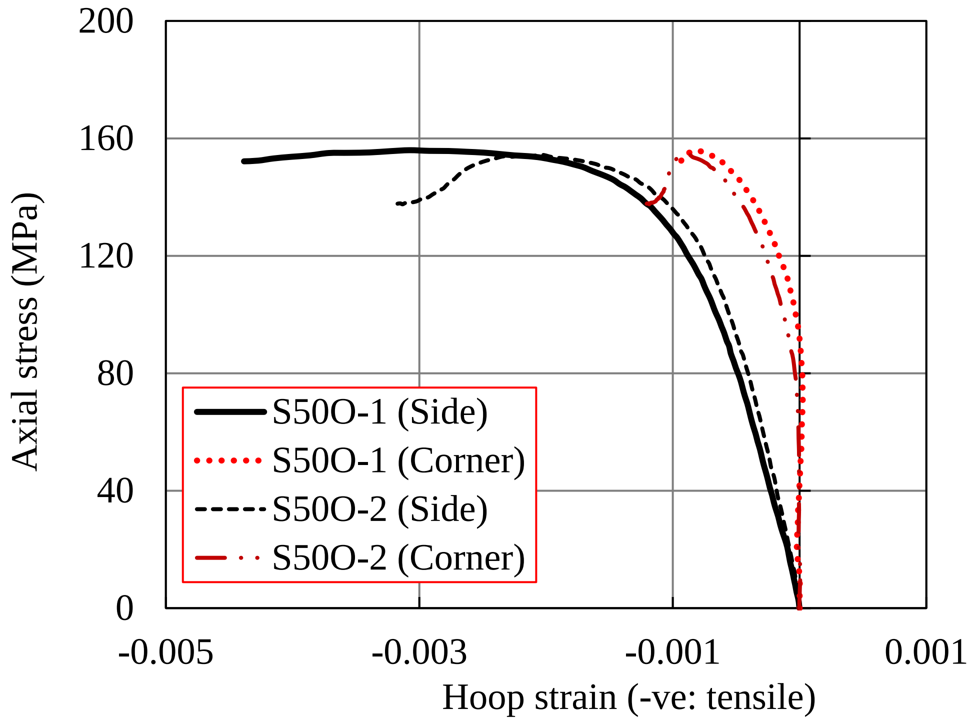

(b) Measured cylinder strength - 80 MPa

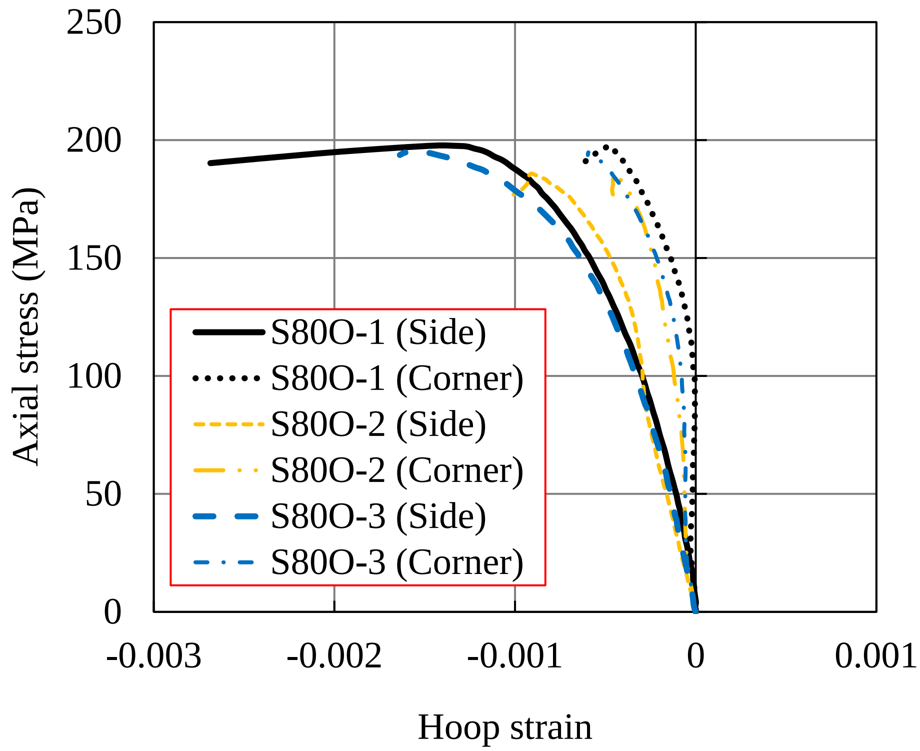

(c) Measured cylinder strength - 112 MPa

Figure 6. Axial stress-hoop strain relationship of octagonal STCC specimens

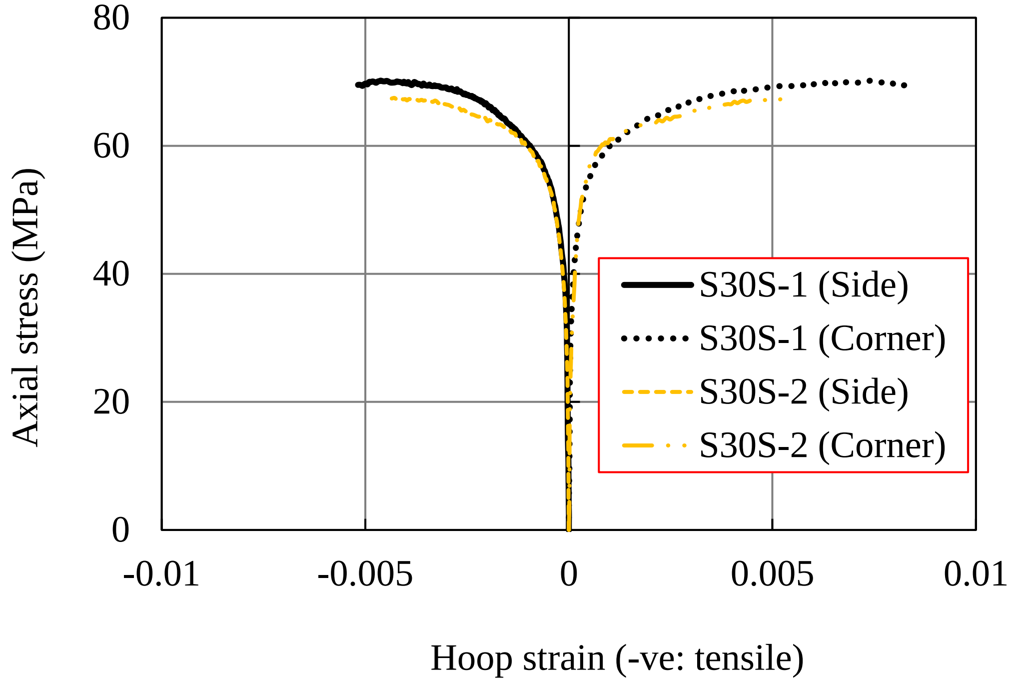

(a) Measured cylinder strength - 38 MPa

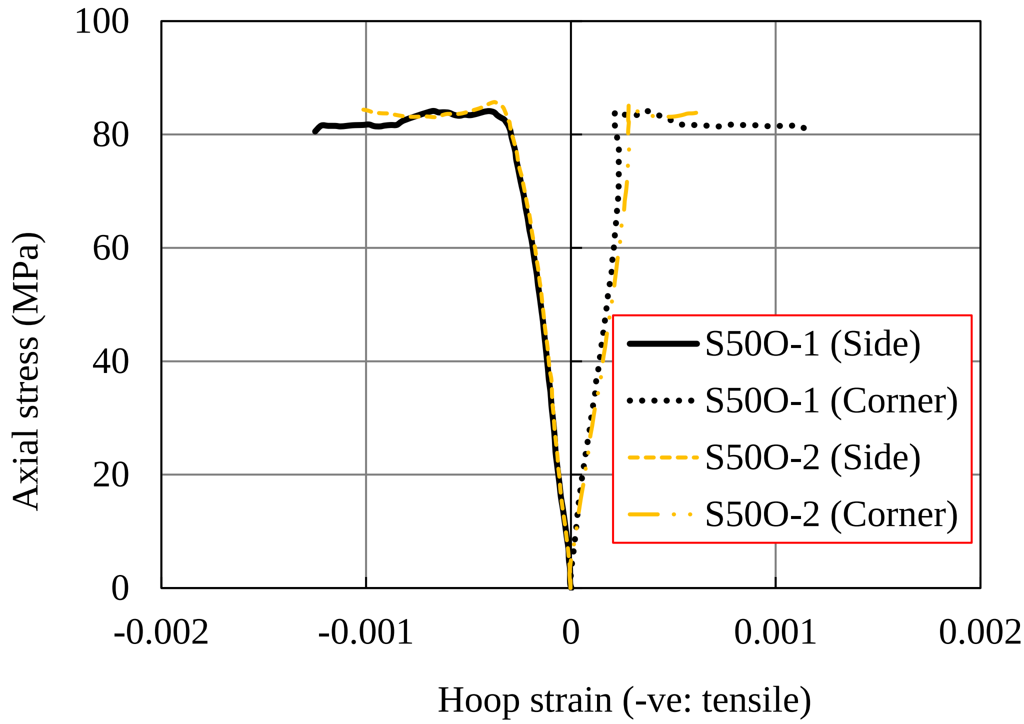

(b) Measured cylinder strength - 80 MPa

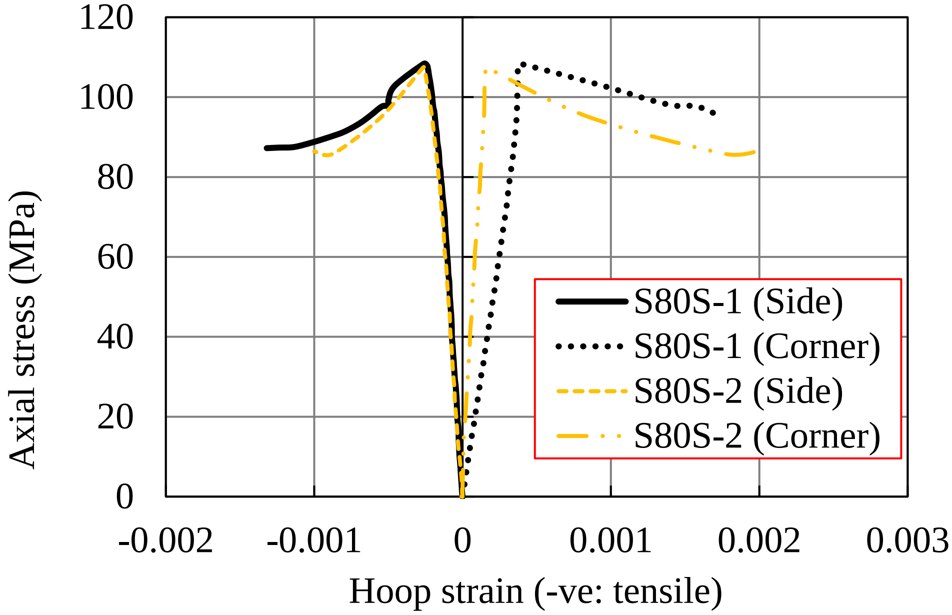

(c) Measured cylinder strength - 112 MPa

Figure 7. Axial stress-hoop strain relationship of square STCC specimens

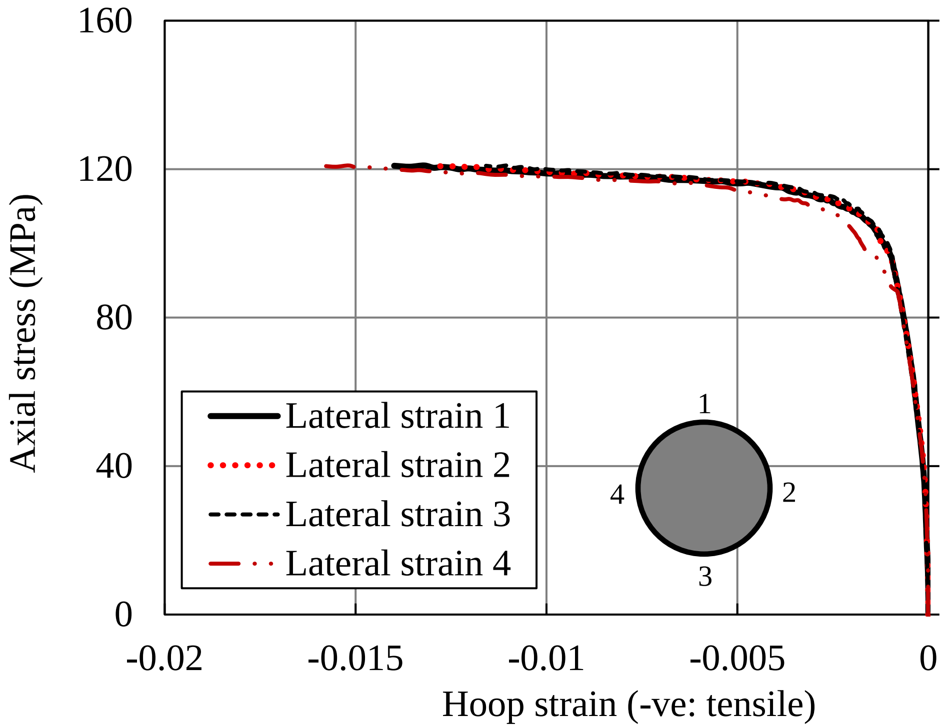

(a) S30C-1

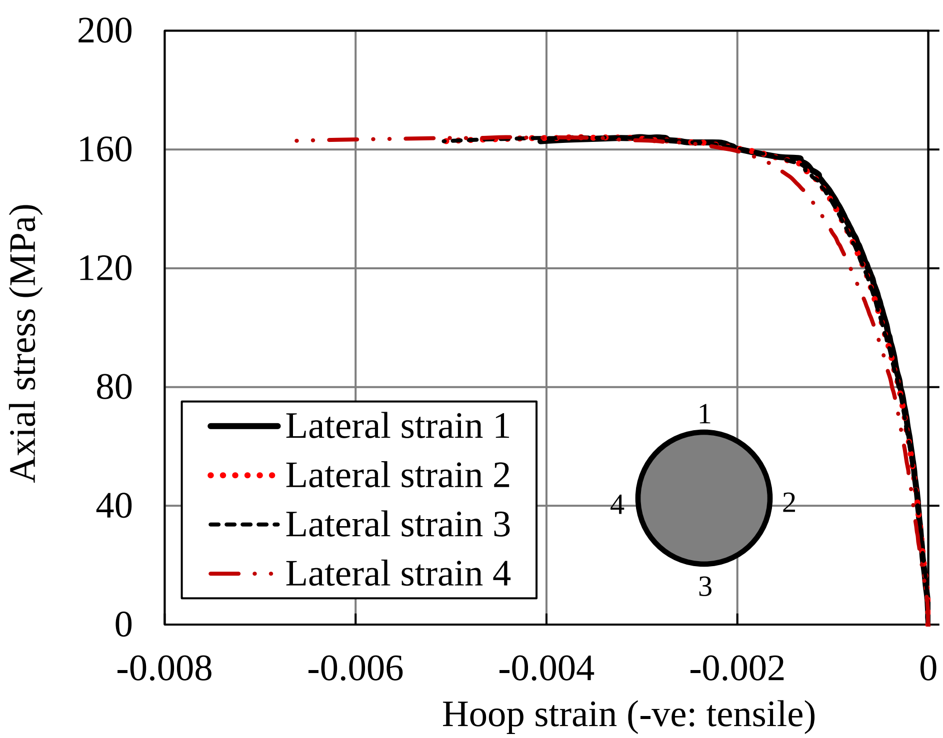

(b) S50C-1

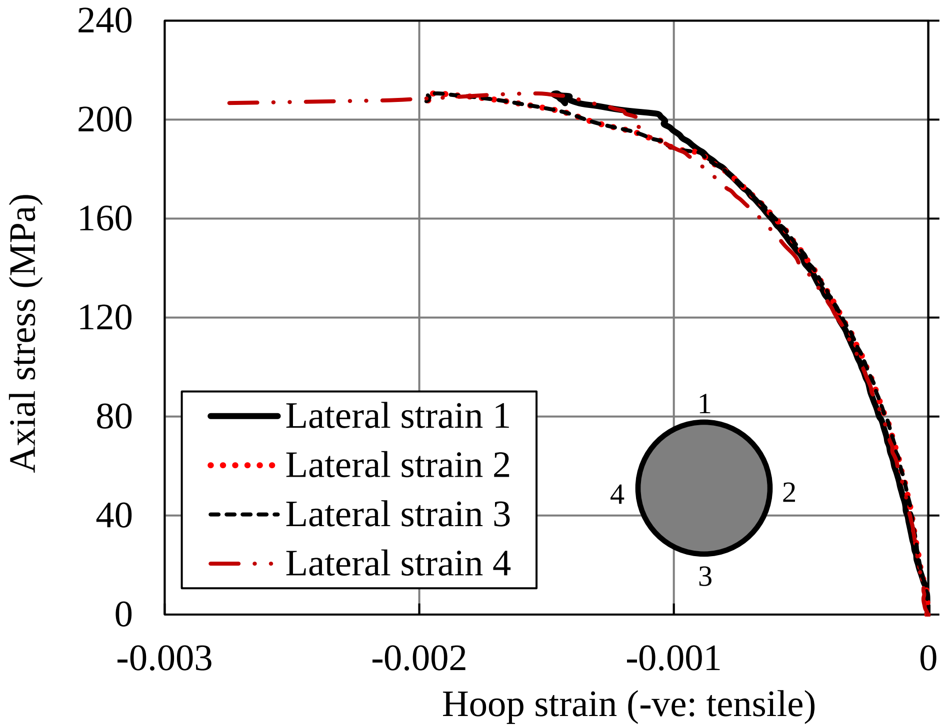

(c) S80C-1

Figure 8. Axial stress-hoop strain relationship of circular STCC specimens

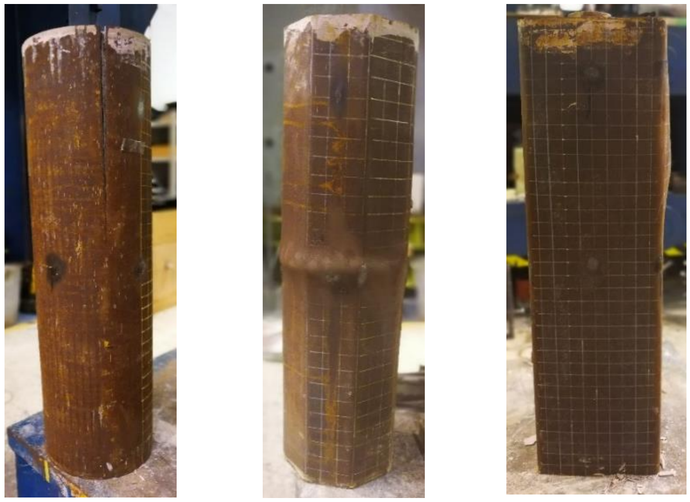

S30C-1 S30O-2 S30S-1

Figure 9. Failure mode of STCC specimens

Figure 10. Failure mode of concrete core of specimens S30O-2

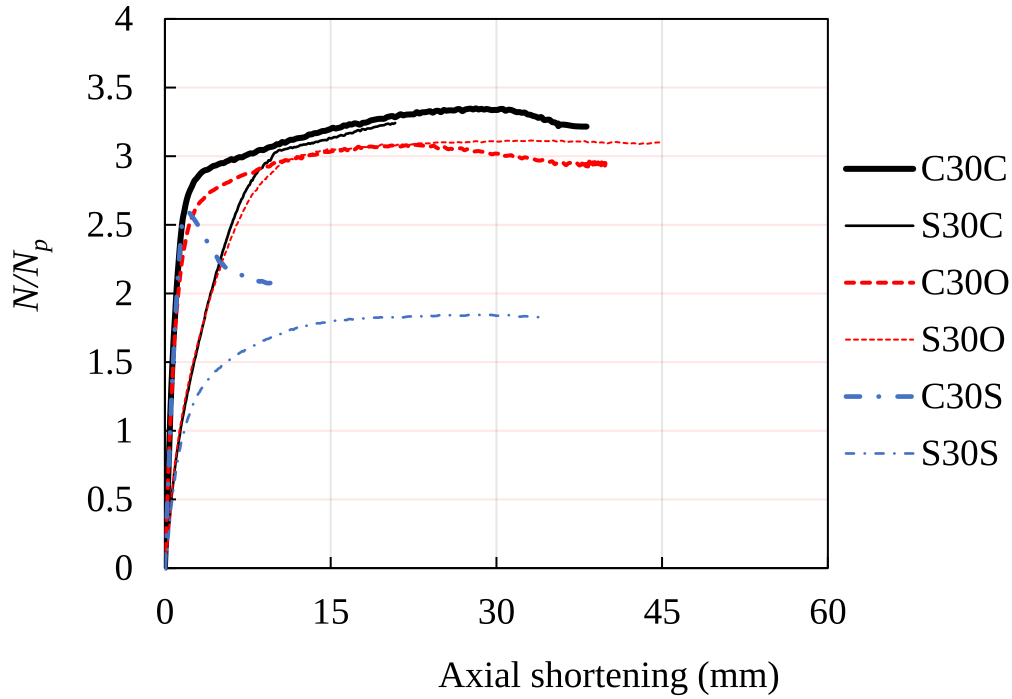

(a) Measured cylinder strength - 38 MPa

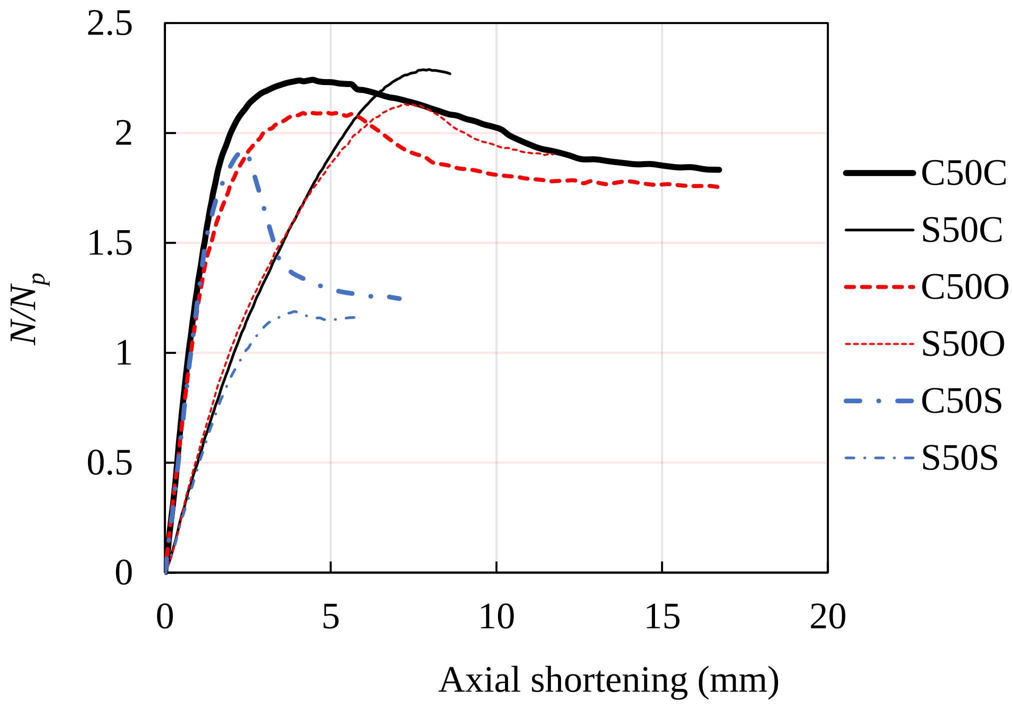

(b) Measured cylinder strength - 80 MPa

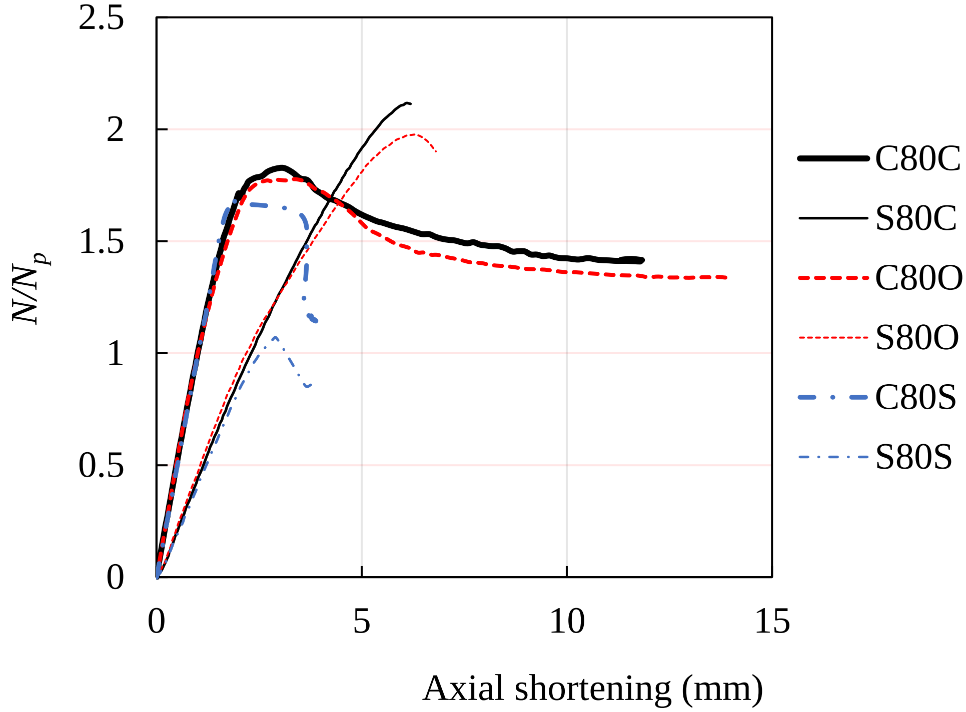

(c) Measured cylinder strength - 112 MPa

Figure 11. Comparison of axial load-axial shortening curves of STCC and CFST specimens.

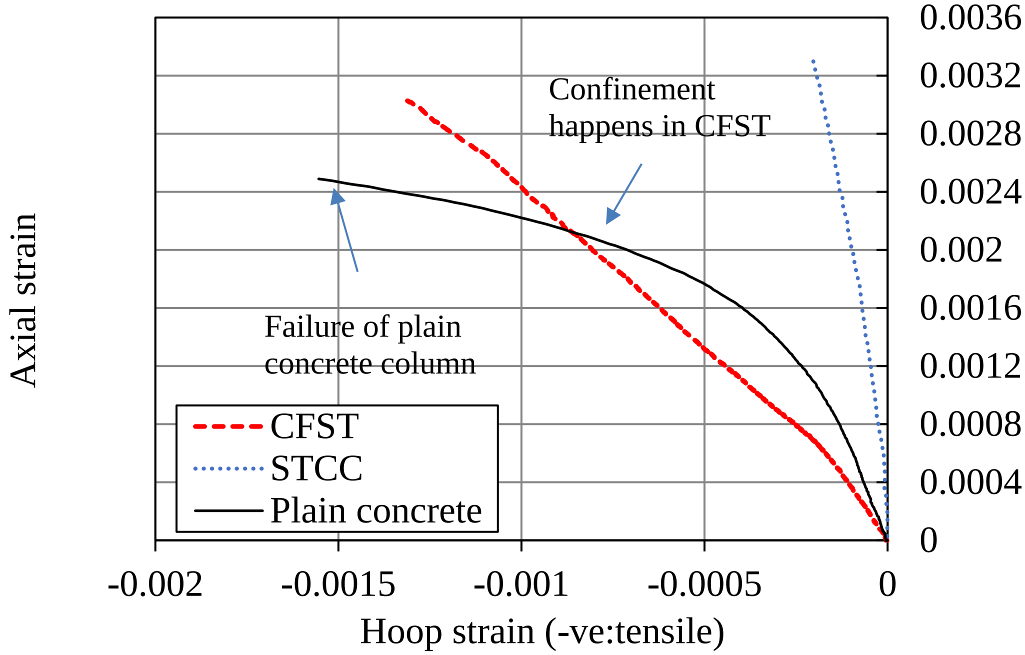

(a) Measured cylinder strength - 38 MPa

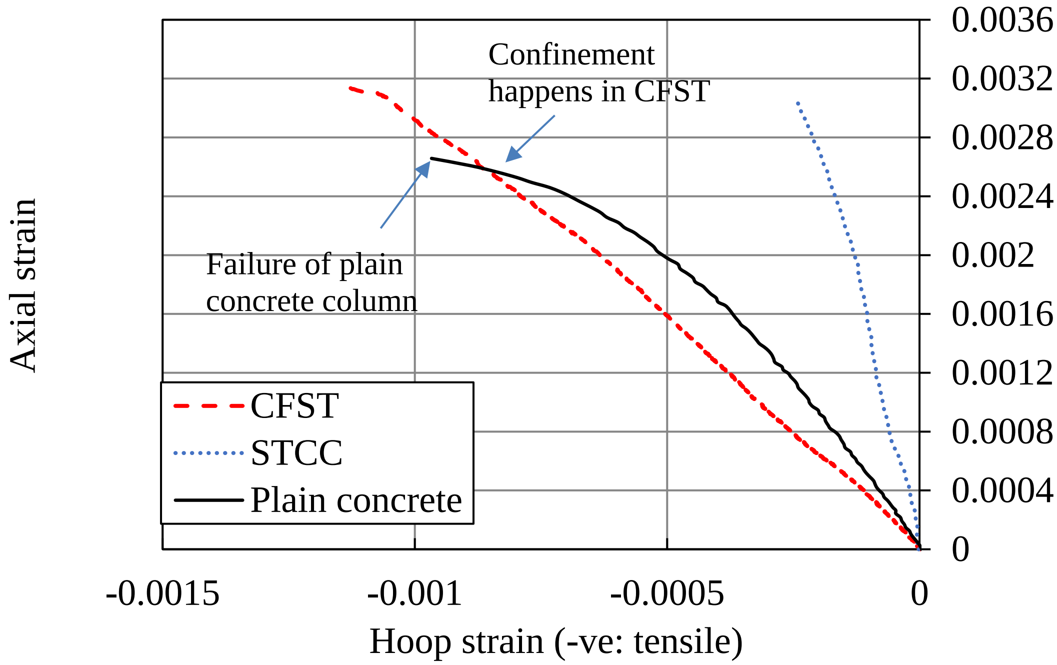

(b) Measured cylinder strength - 80 MPa

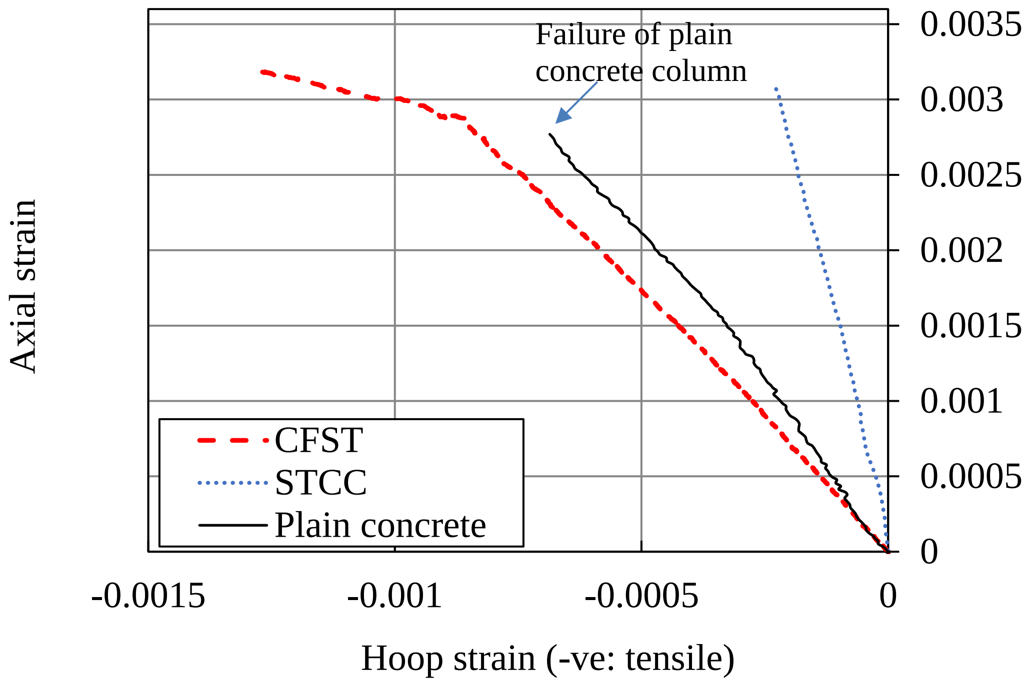

(c) Measured cylinder strength - 112 MPa

Figure 12. Lateral-axial strain of circular STCC, CFST and plain concrete specimens

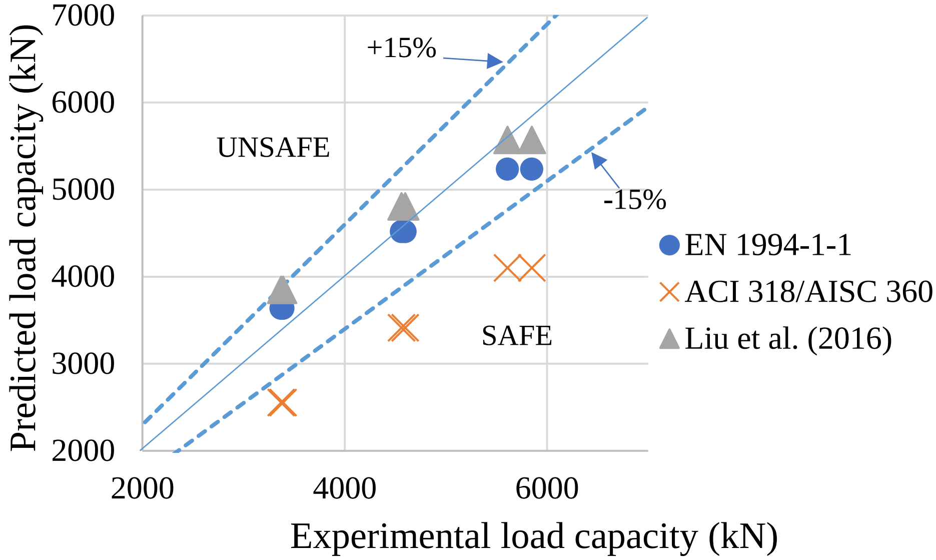

(a) Circular specimens

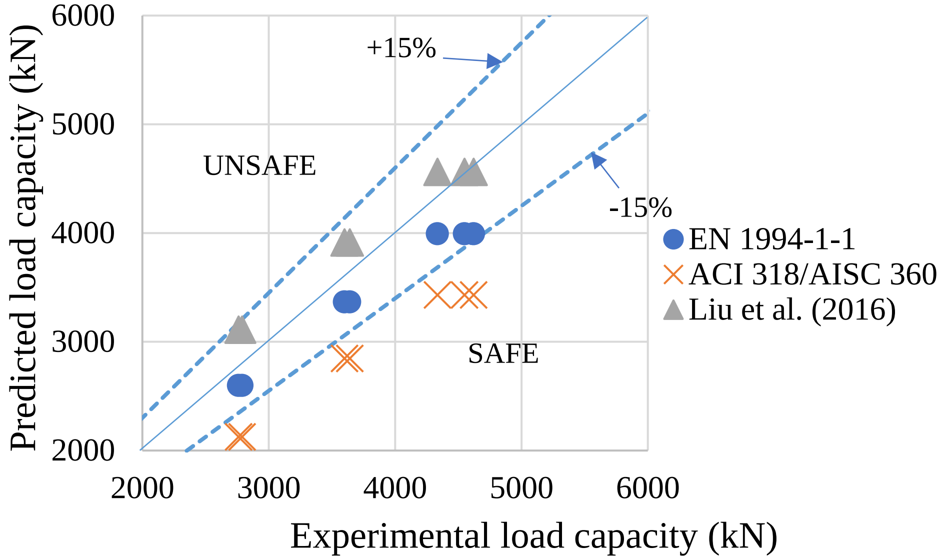

(b) Octagonal specimens

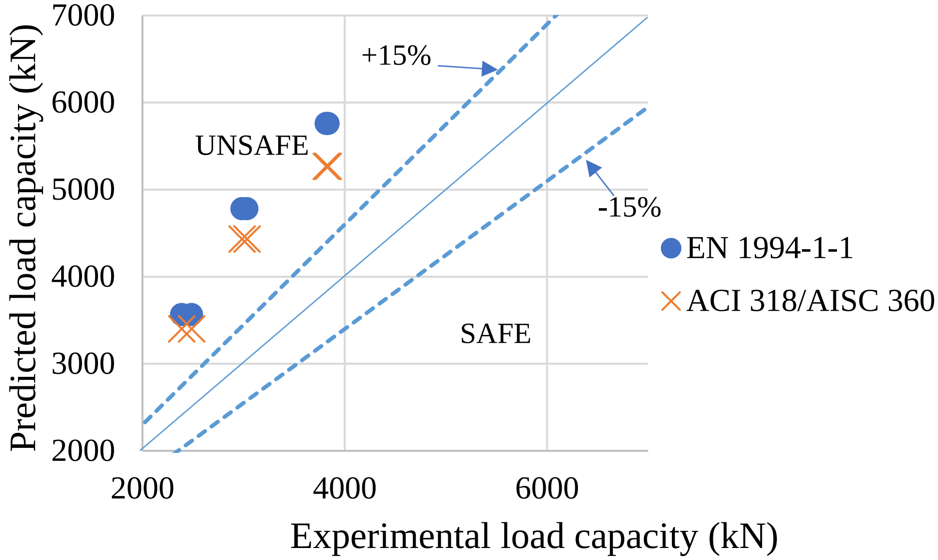

(c) Square specimens

Figure 13. Assessment results of design method for STCC specimens

Table 1. Cross-sectional dimension of the specimens

Cross-section	*D* (mm)	*B* (mm)	*b* (mm)	*t* (mm)	*L* (mm)	*L/D or L/B*	*D*/*t* or *b*/*t*
Octagonal	178	74	60	5.6	695	3.9	31.8 or 10.7
Circular	200	-	-	6.0	695	3.5	33.3
Square	-	200	179	6.0	695	3.5	29.8

Table 2. Material properties of STCC specimens

Component				
Steel tube	Cross-section	f_y (MPa)	f_u (MPa)	*E* (MPa)
	Circular	451	577	215000
	Octagonal	413	521	214000
	Square	485	584	217000
Concrete	Concrete grade	f_{co} (MPa)	$f_{co,c}$ (MPa)	*E* (MPa)
	C25/30	38	38	27600
	C50/60	80	72	35100
	C80/95	112	100	40400

Table 3. Result of STCC stub column tests

Specimens	f_y (MPa)	f_{co} (MPa)	ξ	$N_{u,s}$ (kN)	N_p (kN)	$N_{u,s}/N_p$
S30C-1	451	38	1.54	3372	1045	323%
S30C-2	451	38	1.54	3390	1045	324%
S30O-1	413	38	1.52	2789	885	315%
S30O-2	413	38	1.52	2761	885	312%
S30S-1	485	38	1.68	2487	1343	185%
S30S-2	485	38	1.68	2388	1343	178%
S50C-1	451	80	0.73	4598	1991	231%
S50C-2	451	80	0.73	4561	1991	229%
S50O-1	413	80	0.71	3641	1689	216%
S50O-2	413	80	0.71	3600	1689	213%
S50S-1	485	80	0.79	2986	2551	117%
S50S-2	485	80	0.79	3034	2551	119%
S80C-1	451	112	0.53	5609	2756	204%
S80C-2	451	112	0.53	5850	2756	212%
S80O-1	413	112	0.51	4622	2333	198%
S80O-2	413	112	0.51	4335	2333	186%
S80O-3	413	112	0.51	4550	2333	195%
S80S-1	485	112	0.57	3836	3541	108%
S80S-2	485	112	0.57	3818	3541	108%

Table 4. Comparison of load capacity between STCC and CFST specimens

Specimens	f_{co} (MPa)	$N_{u,s}$ or $N_{u,c}$ (kN)	$N_{u,s}/N_{u,c}$
C30C	38	3511	0.96
S30C	38	3381	
C30O	38	2707	1.03
S30O	38	2775	
C30S	38	3470	0.70
S30S	38	2438	
C50C	80	4443	1.03
S50C	80	4580	
C50O	80	3546	1.02
S50O	80	3621	
C50S	80	4947	0.61
S50S	80	3010	
C80C	112	5070	1.13
S80C	112	5730	
C80O	112	4185	1.08
S80O	112	4502	
C80S	112	6192	0.62
S80S	112	3827	

Table 5. Assessment results on STCC design formulas

Specimens	Eurocode 4/Zhu and Chan [11]		ACI/AISC		Liu *et al.* [10]	
	N_d (kN)	$N_d/ N_{u,s}$	N_d (kN)	$N_d/ N_{u,s}$	N_d (kN)	$N_d/ N_{u,s}$
S30C-1	3637	1.079	2651	0.786	3849	1.141
S30C-2	3637	1.073	2651	0.782	3849	1.135
S50C-1	4518	0.983	3548	0.772	4807	1.046
S50C-2	4518	0.991	3548	0.778	4807	1.054
S80C-1	5235	0.933	4286	0.764	5572	0.993
S80C-2	5235	0.895	4286	0.733	5572	0.953
AVG.		*0.992*		*0.769*		*1.054*
S.D.		*0.074*		*0.019*		*0.075*
S30O-1	2598	0.932	2126	0.762	3112	1.116
S30O-2	2598	0.941	2126	0.770	3112	1.127
S50O-1	3366	0.924	2847	0.782	3914	1.075
S50O-2	3366	0.935	2847	0.791	3914	1.087
S80O-1	3993	0.864	3431	0.742	4562	0.987
S80O-2	3993	0.921	3431	0.791	4562	1.052
S80O-3	3993	0.878	3431	0.754	4562	1.003
AVG.		*0.914*		*0.772*		*1.055*
S.D.		*0.032*		*0.020*		*0.053*
S30S-1	3564	1.433	3400	1.367	-	-
S30S-2	3564	1.492	3400	1.424	-	-
S50S-1	4780	1.601	4433	1.485	-	-
S50S-2	4780	1.575	4433	1.461	-	-
S80S-1	5759	1.501	5268	1.373	-	-
S80S-2	5759	1.508	5268	1.380	-	-
AVG.		*1.518*		*1.415*		
S.D.		*0.061*		*0.050*		